WATER RESOURCES RESEARCH, VOL. 37, NO. 5, PAGES 1113–1128, MAY 2001

Tracer tests in a fractured dolomite
1. Experimental design and observed tracer recoveries

Lucy C. Meigs
Geohydrology Department, Sandia National Laboratories, Albuquerque, New Mexico

Richard L. Beauheim
Repository Performance and Certification Department, Sandia National Laboratories, Albuquerque, New Mexico

Abstract. A series of tracer tests has been conducted in a 7-m-thick fractured dolomite at two sites in southeastern New Mexico. The tests were designed to evaluate transport processes, especially matrix diffusion, in fractured, permeable media. Both single-well injection-withdrawal (SWIW) and multiwell convergent flow (MWCF) tests were conducted. Seventeen different organic tracers (the fluorobenzoic and chlorobenzoic acids) and iodide were used as conservative tracers for the tests. The MWCF tests included repeated tracer injections while pumping the central well at different rates, injection of tracers with different aqueous diffusion coefficients, and injection of tracers into both the full and partial formation thickness. This paper describes the tracer test sites and aquifer characteristics, the experimental methods, and the tracer data produced. The tracer test results provide a high-quality data set for a critical evaluation of the conceptual model for transport. Both the SWIW and MWCF tracer test data showed gradual mass recovery and breakthrough (or recovery) curve tailing consistent with matrix diffusion. However, the SWIW recovery curves did not display the -1.5 log-log slope expected from a conventional double-porosity medium with a single rate of diffusion. The breakthrough curves from MWCF tests conducted at two different pumping rates showed similar peak heights, which is also not what was expected with a conventional double-porosity model. However, the peak heights were different for two tracers with different aqueous diffusion coefficients that were injected simultaneously in one test, consistent with the effects of matrix diffusion. The complexity of the tracer test results suggests that a simple double-porosity conceptual model for transport in the Culebra with a single rate of diffusion is overly simplistic.

1. Introduction

Matrix diffusion is recognized as a potentially important process in the transport of solutes in the subsurface [e.g., *Neretnieks*, 1980; *Maloszewski and Zuber*, 1993; *Wood*, 1996]. Understanding diffusive mass transfer between high-permeability, advection-dominated domains and low-permeability, diffusion-dominated domains can be important for a variety of problems including the following: (1) predicting and accomplishing aquifer restoration [e.g., *National Research Council*, 1994; *Wood*, 1996]; (2) predicting the migration, spread, dilution, and retardation of both natural solutes and contaminants in the subsurface; [e.g., *Foster*, 1975; *Neretnieks*, 1981; *Bradbury et al.*, 1982]; and (3) designing and assessing the safety of nuclear waste repositories where large immobile zones may impede the release of radioactivity to the accessible environment [e.g., *Neretnieks*, 1980, 1993; *Lever et al.*, 1983; *Wels et al.*, 1996; *Meigs et al.*, 1997].

Most of the quantitative studies of diffusion processes have been laboratory studies [e.g., *Grisak et al.*, 1980; *Moreno et al.*, 1985; *Skagius and Neretnieks*, 1986, 1988; *Wood et al.*, 1990; *Ball and Roberts*, 1991; *Schackelford*, 1991; *Byegård et al.*, 1998; *Tidwell et al.*, 2000]. The relatively slow rates of diffusion, especially for hard rocks such as granite, make quantifying the effects of matrix diffusion difficult in the field. However, several field studies have provided valuable insights into matrix diffusion processes [e.g., *Abelin et al.*, 1991; *Jones et al.*, 1992; *Novakowski and Lapcevic*, 1994; *Moench*, 1995; *Hadermann and Herr*, 1996; *Volckaert and Gautschi*, 1997].

To improve our understanding of matrix diffusion processes, a series of tracer tests has recently been conducted in a fractured dolomite at the Waste Isolation Pilot Plant (WIPP) site in southeastern New Mexico (Figure 1). A goal of this study was to conduct well-controlled tracer tests to produce a detailed and accurate database for evaluation of advective and diffusive transport processes in fractured, saturated, permeable media. Although past studies have provided valuable insights into diffusion processes, this is one of the first field tracer test studies that is primarily focused on providing an extensive data set to evaluate matrix diffusion processes.

The purpose of this paper is to describe the recent tracer tests, including the background of the study, a description of the test sites, characteristics of the fractured dolomite, experimental methods used, the results of the tests, and simple conclusions and discussion. Additional papers in this series [*Haggerty et al.*, this issue; *McKenna et al.*, this issue] provide numerical analyses and detailed interpretation of a portion of the tracer test results. Additional details on the tracer tests described in this paper, including the tracer test data, are given

Paper number 2000WR900335.
0043-1397/01/2000WR900335$09.00

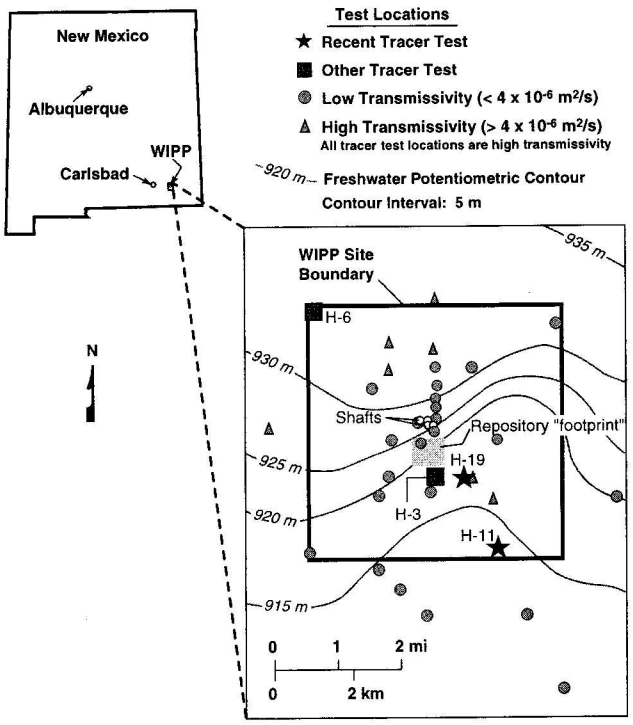

Figure 1. Location of Waste Isolation Pilot Plant (WIPP) site and H-11 and H-19 multiwell sites ("hydropads").

by *Meigs et al.* [2000]. Electronic versions of the data sets are available from the AGU.[1]

2. Background

The tracer tests described in this paper were conducted in the Culebra Dolomite Member of the Rustler Formation at the WIPP site. The WIPP is a repository for transuranic wastes constructed 655 m below ground surface in bedded, Permian-age halite deposits in southeastern New Mexico, United States of America. Site characterization studies at the WIPP site have shown that if radionuclides were to be released from the repository through inadvertent human intrusion and introduced into other geologic formations, groundwater transport through the Culebra would be the most significant pathway to the accessible environment [*U.S. Department of Energy*, 1996]. The Culebra is a 7-m-thick, variably fractured dolomite with massive and vuggy layers lying approximately 440 m above the WIPP repository. Convergent flow tracer tests using conservative tracers were conducted within the Culebra at three "hydropads" (multiple-well sites), designated H-3, H-6, and H-11 (Figure 1), between 1981 and 1988. These tests showed rates and amounts of solute transport to be strongly dependent on flow direction and suggested that a physical retardation mechanism was affecting transport [*Jones et al.*, 1992].

Jones et al. [1992] interpreted these tests using a homogeneous, one-dimensional (radial), conventional (i.e., one rate of diffusion), double-porosity continuum model with three orthogonal, equally spaced fracture sets. The simulations suggest that the observed transport behavior can be explained by a combination of anisotropy in horizontal hydraulic conductivity and matrix diffusion. The simulations also demonstrated that the tailing observed in the breakthrough curve data could not be adequately represented using a homogeneous single-porosity model. However, independent reviewers of the interpretations questioned the assumption that matrix diffusion was the primary or sole mechanism causing physical retardation during these tests [e.g., *Hautojärvi and Vuori*, 1992]. They suggested that other processes in addition to matrix diffusion, such as channeling caused by variations in fracture apertures or delayed release of tracer from the injection wells to the formation, may have contributed to the long tails observed in the tracer breakthrough curves.

As a result of criticism from a variety of regulatory and review groups a series of additional tests was designed and implemented to address specific issues. The tests were conducted at both the H-11 hydropad and a new seven-well site, the H-19 hydropad (Figure 1). The objectives of the tracer tests were to collect detailed and accurate data sets under carefully controlled conditions to test the validity of the double-porosity conceptual model and evaluate the appropriate transport parameters. In addition, tracer tests and hydraulic tests were designed to evaluate the extent to which heterogeneity, anisotropy, layering, and the scale of testing affect flow and transport.

3. Culebra Characteristics and Site Description

Within the 41.4-km^2 area of the WIPP site, 44 wells and four shafts penetrate the Culebra dolomite (Figure 1), which is located about 230 m below land surface. In the vicinity of the WIPP site the Culebra is the most transmissive unit in the Rustler Formation. The Rustler Formation represents the transition between the underlying thick evaporite beds of the Salado Formation (where the WIPP repository has been excavated) and the overlying clastic-dominated continental deposits of the Dewey Lake Redbeds. The Culebra is underlain by a mudstone unit and overlain by an anhydrite unit [*Holt and Powers*, 1988]. The Culebra varies in thickness between approximately 6.7 and 8.9 m in the vicinity of the WIPP site and is approximately 7.4-m thick at both the H-11 and H-19 hydropads [*Holt*, 1997]. The Culebra is a regionally persistent bed within the Rustler and occupies an area of greater than 25,000 km^2 [*Holt*, 1997]. Stratigraphic layering within the Culebra changes little across the WIPP area, apparently as a result of the large size of facies tracts within the Culebra depositional system [*Holt and Powers*, 1988; *Holt*, 1997]. Lateral variations in the Culebra appear to be confined to postdepositional features including fractures and distribution of gypsum cements. *Holt and Powers* [1988] suggest that fracture intensity in the Culebra increases from east to west across the WIPP site.

On the basis of shaft descriptions [*Holt and Powers*, 1984, 1986, 1990], core descriptions [*Holt and Powers*, 1988; *Holt*, 1997], and borehole video logs, four distinct Culebra units (CU) can be identified (Figure 2) in the subsurface across the entire WIPP area [*Holt*, 1997]. The uppermost unit in the Culebra, CU-1, consists primarily of well-indurated microcrystalline dolomite and is more massively bedded than the underlying units. Porosity in the well-indurated dolomite is primarily intercrystalline in nature. Fractures are less common in CU-1 than in lower units and usually appear to be bedding-plane

[1]Supporting material is available via Web browser or via Anonymous FTP from ftp://kosmos.agu.org, directory "apend" (Username = "anonymous", Password = "guest"); subdirectories in the ftp site are arranged by paper number. Information on searching and submitting electronic supplements is found at http://www.agu.org/pubs/esupp about html.

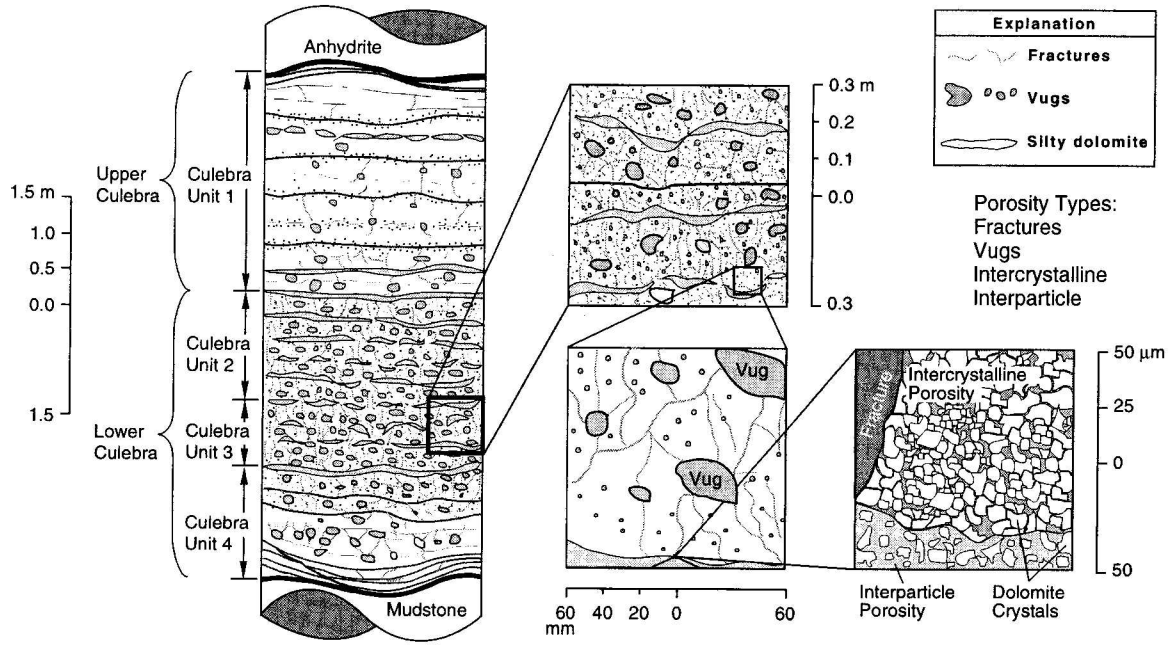

Figure 2. Schematic of vertical variations in Culebra lithologies and porosity types [from *Holt*, 1997].

separations. Small vugs are common in the upper Culebra and frequently occur in zones parallel to stratification. A portion of the vugs and fractures are typically filled with gypsum. CU-1 has an average thickness across the site area of approximately 3.0 m. The Culebra units below CU-1, especially CU-2 and 3, are typically more intensely fractured, have more vugs, and contain interbeds of poorly indurated dolomite. The intensely fractured nature of CU-2 and CU-3 results in very poor core recovery of these two units at many locations. Where core has been recovered (e.g., H-19), portions of it often have a jigsaw-puzzle-like appearance with fractures spaced less than a centimeter to several centimeters apart. Many of the fracture surfaces display dark brown or orange staining suggestive of current or past fluid flow. Vugs in the lower Culebra range in size from a millimeter to a few centimeters and are often connected by microfractures. The vugs are often partially filled with poorly indurated dolomite or gypsum. The poorly indurated dolomite is also referred to as silty dolomite because it is composed of poorly cemented clay- to silt-sized dolomite. The poorly indurated dolomite has a higher interparticle porosity and permeability than the well-indurated dolomite that makes up most of the Culebra. CU-4 is less intensely fractured than CU-2 and CU-3 and has more clearly defined bedding planes that are undulatory in nature. CU-2 and CU-3 combined have an average thickness of 2.8 m across the WIPP area, and CU-4 has an average thickness of 1.6 m. At both the H-11 and H-19 hydropads the lower three units have a combined thickness of about 4.4 m (Table 1). For a more complete description of Culebra lithologies and porosity variations, see *Holt* [1997].

The different porosity types described above and shown graphically in Figure 2 each have a range of permeabilities associated with them. On the time and length scales of our tracer tests, tracer(s) accesses some of this porosity primarily by advection and other portions of the porosity primarily by diffusion. Hence we use the expressions "advective porosity" and "diffusive porosity" to denote the portions of the porosity in which the different processes are dominant. Note that this distinction relies to some degree on the contrast in permeability between different porosity types. Where fracture permeabilities are low, the permeability of the interparticle porosity in the poorly indurated dolomite may be of similar magnitude, so that advection occurs in both porosity types. Where fracture

Table 1. Properties of the Culebra Dolomite at the H-11 and H-19 Hydropads

	H-11 Hydropad	H-19 Hydropad
Field transmissivity (full Culebra), m^2/s	4.7×10^{-5}	6.8×10^{-6}
Thickness of full Culebra, m	7.4	7.4
Thickness of lower Culebra, m	4.4	4.4
Mean and standard deviation of log of core hydraulic conductivity,[a] m/s	-8.40 ± 0.99 (10)[b]	-9.08 ± 1.12 (20)
Mean and standard deviation of core porosity[a]	0.16 ± 0.07 (10)	0.15 ± 0.06 (21)
Mean and standard deviation of core formation factor[a]	66 ± 37 (4)	110 ± 80 (21)
Mean and standard deviation of calculated tortuosity[a]	0.11 ± 0.02 (4)	0.09 ± 0.04 (21)

[a]Mean is the arithmetic average.
[b]Numbers in parentheses denote number of samples.

permeabilities are high, the interparticle porosity may play only a diffusive role. Thus whether a particular porosity type is considered advective or diffusive depends on the properties of the other porosity types at any given location. The advective and diffusive porosities together make up the total interconnected porosity commonly measured in core tests.

The fractures observed in the Culebra differ from the common conceptualization of fractures based largely on fracturing in crystalline rocks. Fractures in crystalline rock are often related to regional tectonic forces and tend to be relatively planar, persist over distances of meters to tens of meters, occur in parallel sets with regular spacings, and have definable orientations (strike and dip). In contrast, regional or local tectonic activity has not caused significant fracturing within the Culebra. The Culebra has primarily fractured in response to differential unloading, dissolution of evaporites from above or below the Culebra, and dissolution of fillings within large vugs and/or zones of vugs in the Culebra [*Beauheim and Holt*, 1990]. The majority of the fractures in the Culebra are subvertical and occur within vuggy zones in CU-2 and CU-3. These fractures usually extend from vug to vug [*Holt and Powers*, 1990], over distances of millimeters to centimeters, with no preferred orientation. Horizontal fractures, parallel to bedding planes, occur throughout the Culebra. These bedding-plane separations were probably caused by stress relief accompanying the erosion of overburden or dissolution of overlying evaporites. Bedding-plane separations have greater lateral extent within the upper Culebra (CU-1) than in the lower Culebra units where more soft-sediment deformation has occurred, disrupting bedding planes. Similarly, high-angle subvertical fractures locally persist vertically for nearly 1 m within the more massive CU-1 but terminate at bedding-plane separations in the lower Culebra. However, the high-angle fractures in CU-1 are typically filled with gypsum in most locations and have little hydraulic significance. Fracture apertures measured in thin sections are highly variable, even in individual fractures, and range from <10 to 500 μm [*Holt*, 1997]. West and south of the WIPP site, the dominant cause of fracturing in the Culebra is collapse following dissolution of the underlying Salado Formation, which caused more extensive fracturing than is observed at the WIPP site.

In the vicinity of the WIPP site, hydraulic tests indicate that the transmissivity of the Culebra varies by 6 orders of magnitude, which *Beauheim and Holt* [1990] suggest is the result of variations in the relative percentages of open and filled fractures. Where the transmissivity is less than 4×10^{-6} m^2/s, hydraulic tests are best interpreted with a single-porosity-medium conceptualization. Where transmissivities are greater than 4×10^{-6} m^2/s, a double-porosity conceptualization best explains the data [*Beauheim and Ruskauff*, 1998]. Double-porosity hydraulic behavior reflects the dominance of open fractures in determining transmissivity and the dominance of the matrix in determining the storage capacity of the medium [*Gringarten*, 1984]. Variations in transmissivity (heterogeneity) are almost certainly present on the hydropad (tens of meters) scale but are difficult to quantify because the pressure transient created by any type of hydraulic test quickly propagates beyond that scale. As a result, transmissivity values interpreted from hydraulic tests of the Culebra represent average properties over distances of hundreds of meters. No evidence of leakage from overlying anhydrite or underlying mudstone confining beds is seen in Culebra hydraulic tests.

Flow in the Culebra is generally to the south across the WIPP site area [*Crawley*, 1988; *Corbet and Knupp*, 1996], with hydraulic gradients ranging from approximately 0.001 to 0.01 m of fresh water per meter distance (Figure 1). The water in the Culebra at the WIPP site entered the Culebra by vertical leakage through overlying units north and northeast of the site rather than by direct precipitation on Culebra outcrops. This water fell as precipitation on the land surface thousands to tens of thousands of years before entering the Culebra [*Corbet and Knupp*, 1996]. The ultimate discharge point to the south for Culebra waters is uncertain. Calculated Darcy velocities on the WIPP site range from approximately 1×10^{-11} to 2×10^{-9} m/s [*LaVenue et al.*, 1990]. Transmissivities are higher in a zone near the H-3, H-11, and H-19 hydropads than elsewhere in the southern portion of the WIPP site (Figure 1). This high-transmissivity zone is potentially important because it could represent a fast transport path to the site boundary for WIPP contaminants released to the Culebra through inadvertent human intrusion of the repository.

Hydraulic tests at several locations suggest that significant vertical variations in hydraulic properties exist in the Culebra. Cross-hole sinusoidal pumping tests indicate that the permeability of the upper portion of the Culebra (CU-1) is significantly lower than the permeability of the lower Culebra (CU-2, CU-3, and CU-4) at the H-19 hydropad [*Beauheim et al.*, 1997]. Hydrophysical (fluid) logging and pressure responses during drilling also suggest that most flow occurs in the lower portion of the Culebra at H-19 [*Beauheim et al.*, 1997]. The results of a tracer (^{131}I) and temperature survey run at the H-3 hydropad indicated that, within the resolution of the test, all flow was in the lower 3 m of the Culebra [*Mercer and Orr*, 1979]. In addition, most of the fluid observed to come out of the Culebra in the air intake shaft (Figure 1) came from the lower portion of the Culebra [*Holt and Powers*, 1990].

Numerous Culebra core samples have been tested for permeability, porosity, and electrical resistivity formation factor [*Kelley and Saulnier*, 1990; *Holt*, 1997] (See Table 1). At the H-19 and H-11 hydropads the hydraulic conductivity in the horizontal direction of core samples ranges from $\sim 10^{-11}$ to 10^{-7} m/s. The higher values are believed to reflect small fractures in the core. The measured Culebra porosities range from 0.09 to 0.30, and formation factors range from 32 to 392.

An approximation of the tortuous nature of the Culebra pore structure, which affects diffusion rates, can be calculated from the measured formation factors. Tortuosity, τ, is expressed as

$$\tau = 1/F\phi, \tag{1}$$

where F and ϕ are the measured formation factor and total interconnected porosity for a given sample, respectively [*Klinkenberg*, 1951; *Kelley and Saulnier*, 1990]. Table 1 lists the average tortuosity and other property values for cores from the H-11 and H-19 hydropads. The average core hydraulic conductivities are approximately 2 orders of magnitude lower than the hydraulic conductivities calculated by dividing the field transmissivities by the Culebra thickness, showing the importance of fractures at the field scale that are not captured in core tests.

In the vicinity of the WIPP site, Culebra water is a moderate to high ionic strength brine of predominantly sodium chloride composition. Waters from the H-11 and H-19 hydropads are a sodium chloride type brine with Mg/Ca molar ratios of 1.4 and ionic strengths of 2.2 and 1.7, respectively [*Siegel et al.*, 1991; *Meigs and Beauheim*, 2000]. The density of the Culebra brine is

approximately 1.08 and 1.07 g/cm^3 at the H-11 and H-19 hydropads, respectively [*Randall et al.*, 1988; *Meigs and Beauheim*, 2000]. The pH of Culebra brine measured in the field at H-11 and H-19 is between 7.0 and 7.5 [*Siegel and Anderholm*, 1994; *Meigs and Beauheim*, 2000]. Culebra water temperatures typically range from 23° to 27°C [e.g., *INTERA Technologies, Inc.*, 1986; *Stensrud et al.*, 1990].

4. Experimental Design

Two types of tracer tests were conducted: single-well injection-withdrawal (SWIW) tests and multiwell convergent-flow (MWCF) tests. For the SWIW tests, one or two tracers were injected into a well followed by a chaser solution of Culebra brine to displace the tracer(s) from the well bore into the formation. After a pause of 18 hours the well was pumped to recover the tracer(s). The MWCF tests were initiated after pumping for the SWIW tests had created effectively steady state hydraulic gradients on the hydropad. Tracers (and chaser) were injected into the wells surrounding the pumping well and recovered at the pumping well. Numerous benzoic acids were used as conservative (nonreactive) tracers to allow the collection of tracer recovery and breakthrough data from multiple pathways simultaneously.

Numerical simulations by *Tsang* [1995] suggested that a SWIW test is an excellent way of evaluating the importance of matrix diffusion, even in a highly heterogeneous aquifer. Her results show that mass is always recovered much more slowly when matrix diffusion is occurring than when it is not. Because slow mass recovery can also be caused by tracer plume drift under ambient flow conditions [*Lessoff and Konikow*, 1997], the pause period between injection and pumping was kept relatively short (18 hours) for the SWIW tests to minimize drift.

Two features of the MWCF tests were designed to evaluate matrix diffusion. First, after tracers had been injected and recovered while the central well was pumped at one rate, the pumping rate was changed, and new tracers were injected to show the effects of advective residence time on diffusion. Second, two different conservative tracers having different aqueous diffusion coefficients were injected together to show the effects of different amounts of diffusion. Another feature of the MWCF tests was the injection of tracers into packed-off subsections of the Culebra to evaluate the importance of vertical variations in Culebra properties.

5. Experimental Description and Methodologies

Tracer tests were conducted at two locations, the H-11 and the H-19 hydropads. The H-11 hydropad comprises four wells (Figure 3), which were used for a tracer test conducted in 1988 [*Jones et al.*, 1992]. Seven wells were drilled at the H-19 hydropad (Figure 4) in the spring and summer of 1995 using brine and air rotary methods [*Mercer et al.*, 1998]. Wells were located to examine flow paths in multiple directions and maximize the volume of Culebra that could be tested between wells. Fiberglass casing was cemented in the wells from ground surface to within 3 m of the Culebra, and the Culebra intervals were completed as open holes. The Culebra interval of the central well, H-19b0, was drilled to a diameter of approximately 20 cm, and the Culebra intervals of the surrounding wells were drilled to diameters of approximately 15 cm.

After the first four wells were drilled (H-19b0, H-19b2, H-19b3, and H-19b4), preliminary SWIW and MWCF tracer tests were conducted. For the SWIW test, two tracers and chaser were injected over the entire Culebra thickness in H-19b0. Details about the implementation of this SWIW test are given in Table 2. The MWCF test was designed to evaluate transport rates to aid in both siting of the remaining wells and final test design, and it also served as a test of equipment. The test was conducted at a pumping rate of approximately 0.24 L/s, which created hydraulic gradients ranging from 1.4 to 3.0 m of fresh water per meter distance along the three flow paths tested (Table 3). This tracer test revealed that the time to breakthrough curve peak arrival was significantly slower for two pathways (H-19b2 to H-19b0 and H-19b4 to H-19b0) than for pathways at previous MWCF test sites (i.e., H-3, H-6, and H-11) (Figure 1). As a result, the last two wells, H-19b6 and H-19b7, were drilled much closer to H-19b0 than had been originally planned (see *Beauheim* [2000b] for additional details). The results of the preliminary H-19 four-well MWCF

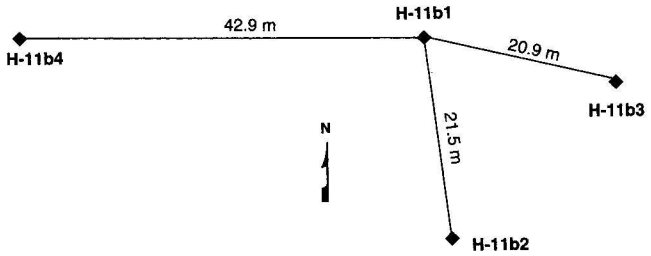

Figure 3. Downhole (Culebra) well locations at the H-11 hydropad.

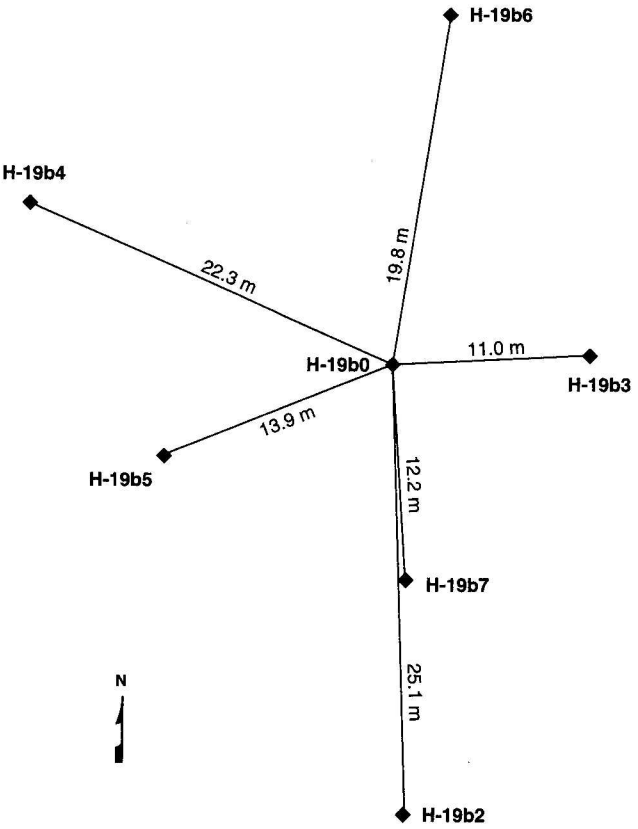

Figure 4. Downhole (Culebra) well locations at the H-19 hydropad.

Table 2. Tabulated Information on the SWIW Tracer Tests at the H-11 and H-19 Hydropads

Test	Pumping Rate, L/s	Injection Date	Culebra Interval	Pause Length, hour	Tracer[a]	Tracer Concentration,[b] g/L	Calculated Aqueous Diffusion Coefficient,[c] m^2/s	Tracer-Injection Rate, L/s	Injected Tracer Volume, L	Chaser-Injection Rate,[d] L/s	Injected Chaser Volume, L	Time to Final Sample, days	Calculated Mass Recovered (Fraction)
H-11 SWIW (H-11b1)	0.22	Feb. 6, 1996	full	17.7	2,4-DCBA	8.07 ± 0.40	7.3×10^{-10}	0.12	996	0.13	1920	50	0.98
		Feb. 6, 1996	full	17.7	3,4-DFBA	5.02 ± 0.32	8.2×10^{-10}	0.13	1010	0.12	910	50	0.97
H-19 SWIW 1 (H-19b0)	0.24	June 15, 1995	full	17.6	2,4-DCBA	4.94 ± 0.21	7.3×10^{-10}	0.13	997	0.13	2020	32	0.95
		June 15, 1995	full	17.6	o-TFMBA	1.91 ± 0.04	7.4×10^{-10}	0.13	1005	0.13	1015	32	0.98
H-19 SWIW 2 (H-19b0)	0.27	Dec. 21, 1995	lower	17.7	2,4-DCBA	5.97 ± 0.17	7.3×10^{-10}	0.12	849	0.12	1697	26	0.94

[a]Tracers are as follows: 2,4-DCBA, 2,4-dichlorobenzoic acid; 3,4-DFBA, 3,4-difluorobenzoic acid; and o-TFMBA, ortho-trifluoromethylbenzoic acid.
[b]The concentrations listed result in an initial increase in solution density of between 0.2 and 0.8%, which will decrease rapidly because of mixing with water in the borehole and formation. The temperature of injected solution was colder than the formation water by as much as 10°–20°C for the winter injections and was probably slightly warmer for the summer injections. These temperature differences will also affect the density and viscosity differences between the injected and ambient fluids. Calculations suggest temperature effects should be small and will dissipate rapidly.
[c]Aqueous diffusion coefficient is calculated using the Hyduk and Laudie method as described by *Tucker and Nelken* [1982].
[d]For June 15, 1995, and February 6, 1996, tests, injection sequence consisted of injection of tracer 1 (2,4-DCBA), followed by tracer 2 (o-TFMBA or 3,4-DFBA), followed by chaser (Culebra brine). For tracer 1 listed above, chaser injection rate and volume are calculated as the rate or volume for injection of both tracer 2 and the chaser fluid.

test are not discussed in this paper. For more information, see *Meigs et al.* [2000].

The final tracer tests at the H-19 hydropad began in December 1995, lasted 120 days, and had four phases: initiation of the SWIW test, round 1 of MWCF injections at the high pumping rate, round 2 of MWCF injections at the high pumping rate, and round 3 of MWCF injections at the low pumping rate. The details of each test phase are tabulated in Tables 2 and 3. The high pumping rate was selected to be slightly below the estimated maximum sustainable rate for the well (about 0.3 L/s). The low pumping rate was selected to be slightly more than half the high pumping rate. The lower rate was selected as a compromise between the desire to maximize the difference in pumping rates and the need to minimize the time to complete the tests. The tracer test began with tracer and chaser (Culebra brine) injection into the lower portion of H-19b0 for the SWIW test, followed by an 18-hour pause before pumping began in H-19b0. After pumping for 5 days, distinct tracers were injected (round 1) into each of the six surrounding wells, with injections over the full Culebra thickness in all wells except H-19b5, in which separate tracers were injected into the upper and lower Culebra. Estimated hydraulic gradients on the H-19 hydropad during this phase of testing ranged from 1.7 to 3.7 m of fresh water per meter distance (Table 3). Approximately 26 days later, distinct tracers were injected (round 2) into the upper and lower Culebra in H-19b3 and H-19b7 and over the full Culebra interval in H-19b5. Hydraulic gradients along these flow paths during this phase of testing ranged from 2.8 to 3.5 m of fresh water per meter distance. After approximately 32 more days, the pumping rate was decreased from 0.25 L/s to 0.16 L/s, and tracer injections were repeated (round 3) over the full Culebra thickness in H-19b3, H-19b6, and H-19b7. Hydraulic gradients along these flow paths ranged from 1.3 to 2.0 m of fresh water per meter distance (Table 3).

The tracer test at the H-11 hydropad began in February 1996, lasted 45 days, and had three phases: initiation of the SWIW test, round 1 of MWCF injections at a low pumping rate (0.22 L/s), and round 2 of MWCF injections at a high pumping rate (0.38 L/s). Tables 2 and 3 tabulate the test details. H-11b1 served as the pumping well and H-11b2 and H-11b3 were used as injection wells. H-11b4 was not used because of poor tracer resolution (low concentrations near the analytical detection limit) and late peak arrival during the 1988 test [*Jones et al.*, 1992]. Hydraulic gradients from H-11b2 and H-11b3 to H-11b1 were approximately 0.31 and 0.30 m of fresh water per meter distance, respectively, during round 1 and were 0.70 and 0.72 m/m, respectively, during round 2 (Table 3). At the H-11 hydropad, tests were terminated earlier than planned because of equipment problems, and tracers were only injected over the full Culebra interval.

During the final H-19 and H-11 tracer tests, transducers in the well casing above the packer isolating the Culebra showed slight pressure declines over the course of the tracer tests in most of the wells, corresponding to potential leaks into the test zones of some tens of liters [*Beauheim*, 2000a]. These small amounts of leakage, if they occurred, could not have measurably affected tracer transport. No evidence of leakage around the packers was observed during the preliminary H-19 tracer test.

5.1. Tracer Selection

During tracer testing, 18 different tracers were used at the H-19 hydropad and seven different tracers were used at the

Table 3. Tabulated Information on the MWCF Tracer Tests at the H-11 and H-19 Hydropads

Test	Pumping Rate, L/s	Path	Injection Date	Average Hydraulic Gradient,[a] m/m	Tracer[b]	Tracer Concentration,[c] g/L	Calculated Aqueous Diffusion Coefficient,[d] m^2/s	Tracer-Injection Rate, L/s	Injected Tracer Volume, L	Chaser-Injection Rate, L/s	Injected Chaser Volume, L	Time to Final Sample, days	Calculated Mass Recovered (Fraction)
H-11 1996	0.22	b2-b1	Feb. 15, 1996	0.31	2,6-DFBA	10.38 ± 0.05	8.2×10^{-10}	0.068	189	0.060	213	41	0.40
round 1		b3-b1	Feb. 15, 1996	0.30	2,3,4,5-TFBA	10.85 ± 0.24	7.9×10^{-10}	0.096	189	0.098	372	41	0.74
H-11 1996	0.38	b2-b1	March 14, 1996	0.70	p-TFMBA	10.78 ± 0.11	7.4×10^{-10}	0.072	189	0.062	213	13	0.21
round 2		b3-b1	March 13, 1996	0.72	2,5-DFBA,	10.30 ± 0.15	8.2×10^{-10}	0.095	190	0.097	373	14	0.56
		b3-b1	March 13, 1996	0.72	NaI	10.87 ± 0.03	18.0×10^{-10}	0.095	190	0.097	373	14	0.53
H-19 1995 (preliminary	0.24	b2-b0	June 19, 1995	1.4	2,3-DFBA	7.30 ± 0.34	8.2×10^{-10}	0.11	246	0.11	246	37	0.54
four-well test)		b3-b0	June 20, 1995	3.0	2,3,4,5-TFBA	7.77 ± 0.27	7.9×10^{-10}	0.15	259	0.14	206	37	0.69
		b4-b0	June 19, 1995	1.6	2,6-DFBA	7.06 ± 0.58	8.2×10^{-10}	0.13	265	0.11	255	37	0.41
H-19 1995–1996	0.27	b2-b0	Dec. 22, 1995	1.7	2,3,4-TFBA	8.18 ± 0.25	8.0×10^{-10}	0.13	202	0.15	154	104	0.88
		b3-b0	Dec. 22, 1995	3.7	m-TFMBA	9.52 ± 0.51	7.4×10^{-10}	0.18	198	0.23	173	104	0.88
		b3-b0	Dec. 22, 1995	3.7	NaI	12.71	18.0×10^{-10}	0.18	198	0.23	173	63	0.80
		b4-b0	Dec. 22, 1995	2.1	3,5-DFBA	8.46 ± 1.95	8.2×10^{-10}	0.12	198	0.12	143	104	0.84
		b5(u)-b0	Dec. 20, 1995	3.0	2,3-DCBA	11.45 ± 0.31	7.3×10^{-10}	0.015	147	0.010	105	106	0.18
		b5(l)-b0	Dec. 20, 1995	3.0	2,5-DCBA	13.49 ± 1.26	7.3×10^{-10}	0.011	149	0.009	65	106	0.84
		b6-b0	Dec. 21, 1995	2.3	2,5-DFBA	9.49 ± 0.13	8.2×10^{-10}	0.12	199	0.12	154	106	0.88
		b7-b0	Dec. 21, 1995	3.3	2,4-DFBA	7.58 ± 0.53	8.2×10^{-10}	0.21	198	0.22	168	105	1.03
H-19 1995–1996	0.25	b3(u)-b0	Jan. 19, 1996	3.5	p-TFMBA	14.13 ± 0.32	7.4×10^{-10}	0.016	132	0.015	69	82	0.13
round 2		b3(l)-b0	Jan. 19, 1996	3.4	o-TFMBA	9.69 ± 0.25	7.4×10^{-10}	0.028	198	0.033	143	82	0.89
		b5-b0	Jan. 19, 1996	2.8	2,4-DCBA	9.85 ± 0.66	7.3×10^{-10}	0.19	199	0.17	169	82	0.83
		b7(u)-b0	Jan. 20, 1996	3.0	PFBA	14.51 ± 0.10	7.7×10^{-10}	0.008	131	0.010	64	81	0.05
		b7(l)-b0	Jan. 20, 1996	3.1	3,5-DCBA	7.67 ± 0.41	7.3×10^{-10}	0.016	197	0.015	139	81	0.90
H-19 1995–1996	0.16	b3-b0	Feb. 22, 1996	2.0	2,3,4,5-TFBA	9.95 ± 0.34	7.9×10^{-10}	0.100	198	0.12	173	48	0.80
round 3		b6-b0	Feb. 22, 1996	1.3	2,4,6-TCBA	9.87 ± 0.35	6.8×10^{-10}	0.070	197	0.068	153	48	0.74
		b7-b0	Feb. 22, 1996	1.8	2,3,6-TFBA	9.54 ± 0.27	8.0×10^{-10}	0.12	199	0.12	168	48	0.91
		b7-b0	Feb. 22, 1996	1.8	NaI	10.68 ± 1.50	18.0×10^{-10}	0.12	199	0.12	168	48	0.88

[a]Meters of fresh water per meter distance are shown.

[b]Tracers are as follows: x,y-DFBA, x,y-difluorobenzoic acid (e.g., 2,6-DFBA is 2,6-difluorobenzoic acid); 2,3,4,5-TFBA, 2,3,4,5-tetrafluorobenzoic acid; m-TFMBA, o-TFMBA, or p-TFMBA, meta-, ortho-, or para-trifluoromethylbenzoic acid; NaI, sodium iodide; x,y,z-TFBA, x,y,z-trifluorobenzoic acid; x,y-DCBA, x,y-dichlorobenzoic acid; PFBA, pentafluorobenzoic acid; and 2,4,6-TCBA, 2,4,6-trichlorobenzoic acid.

[c]The concentrations listed result in an initial increase in solution density of approximately 0.9% for most injections and vary from 0.7% up to ~2% for the cases where a benzoic acid and iodide were coinjected. The density should decrease rapidly mixing with water in the borehole and formation. The temperature of injected solution was colder than the formation water by as much as 10°–20°C for the winter injections and was probably slightly warmer for the summer injections. These temperature differences will also affect the density and viscosity differences between the injected and ambient fluids. Calculations suggest temperature effects should be small and will dissipate rapidly.

[d]Aqueous diffusion coefficients are calculated using the Hyduk and Laudie method as described by *Tucker and Nelken* [1982].

H-11 hydropad. The fluorobenzoic and chlorobenzoic acids were selected as the primary tracers because they behave conservatively and could be chromatographically separated [*Farnham et al.*, 2000a]. Batch tests and field tests previously conducted using several of the benzoic acids [*Benson and Bowman*, 1994; *Bowman and Gibbens*, 1992; *Jones et al.*, 1992] suggested that many of the fluorobenzoic acids should behave conservatively in waters, such as the deep Culebra waters, with low potential for biotransformation and near neutral pH. A series of batch tests was recently conducted using all chlorobenzoic and fluorobenzoic acids used in the H-11 and H-19 tracer tests with crushed Culebra sediment. These tests showed no apparent sorption of the benzoic acids to Culebra sediments over a 90-day period [*Farnham et al.*, 2000a]. Background concentrations of the benzoic acids in Culebra brines were below detection limits (0.01–0.05 mg/L).

For two of the H-19 injections and one H-11 injection, iodide in the form of sodium iodide was injected in addition to the benzoic acid tracer. Iodide was selected because it has a aqueous diffusion coefficient that is approximately 2–3 times higher than those of the benzoic acids and has been shown to behave conservatively in many environments [*Davis et al.*, 1980]. Iodide was also selected because it had a relatively low background concentration (<0.1 mg/L); bromide or chloride could not be used as tracers because their background concentrations are too high in Culebra brine.

5.2. Tracer Mixing and Injection

Culebra brine pumped from the hydropad or a nearby well prior to the tracer test was used to mix the tracer solution and as the chaser fluid. Tracer solutions were mixed in 1135-L (300 gallon) polyethylene containers that were equipped with circulation systems to ensure uniform tracer concentration during injection (see Tables 2 and 3). For most of the multiwell injections, 200 L of a 10-g/L tracer solution were used. On the basis of past tests we estimated that a 2000-g mass of tracer was needed for adequate breakthrough curve definition (i.e., peak concentrations between 2 and 10 mg/L and significant breakthrough curve tails before concentrations dropped below detection). Volumes of chaser solution for the MWCF tests were selected to be approximately 2–3 times the borehole volume to flush tracer from the borehole. For the SWIW tests, larger masses of tracer were used (at lower concentrations) to provide recovery concentrations ranging over several orders of magnitude. For two of the SWIW tests, approximately 1000-L volumes of each of the two tracers and chaser were used so as to be similar to SWIW design calculations by *Tsang* [1995]. For the second SWIW test at H-19, only 850 L of tracer solution followed by 1700 L of chaser solution were injected into the lower portion of the Culebra.

For all tests, tracer solutions were injected using a centrifugal magnetic drive pump to deliver the tracer and chaser solutions from mixing and holding tanks to the wells. Injection rates were constant within ±5% in most cases. The tracer distribution and pumping assemblies used in H-19b0 and H-11b1 for the SWIW and MWCF tests are shown in Figure 5. Tracer injection for the SWIW tests was performed by pumping tracer and chaser downhole through 1.27-cm polyethylene tubing at rates of 0.12 to 0.13 L/s (Table 2). An injection manifold at the top of each injection assembly split the tracer solution into four smaller tubes, through which the tracer was injected at different depths and different radial positions within the Culebra. For the H-11 and preliminary H-19 SWIW tests, tracers were injected over the full thickness of the Culebra (Figures 5a and 5b). For the final H-19 SWIW test, tracers were injected only into the lower Culebra (Figure 5c). Packers were positioned above the top of the Culebra to provide isolation during tracer injection and pumping. During the final H-19 SWIW test, additional packers were set at the base of CU-1 and below the Culebra in H-19b0. The packer at the base of CU-1 was deflated after tracer injection was completed and pumping for tracer recovery had begun.

Figure 6a shows a schematic of the downhole tracer distribution tools used in H-19b2, H-19b4, and H-19b6 during the final MWCF test. Tracer (and chaser) were delivered to the injection manifold through a single 1.27-cm polyethylene tube and then split into four sets of injection ports. Injection port sizes were carefully graded (larger at the bottom than at the top) to provide relatively uniform delivery of tracer to the formation. Somewhat cruder versions of these tools having injection ports of only a single size were used in H-19b2, H-19b3, and H-19b4 during the preliminary H-19 MWCF test. The downhole tracer distribution tools used at the H-11 hydropad were similar to those depicted in Figure 6a except that no packers could be placed at the base of the Culebra because of sloughing of the borehole wall. At each of the three wells closest to H-19b0 (H-19b3, H-19b5, and H-19b7), a tool with two injection assemblies (Figure 6b) was used during the final MWCF test that included a packer that could be inflated in the middle of the Culebra so that distinct tracers could be injected into the upper and lower portions of the Culebra. With the packer deflated, a single tracer could be injected through both injection assemblies simultaneously. Pressures were monitored in all wells throughout the tracer tests.

5.3. Sample Collection and Analysis

At each hydropad, tracer testing began with injection into the pumping well for the SWIW test, followed by an 18-hour pause after which pumping was initiated. Pumping rate fluctuations were minor and did not significantly affect the tracer data [*Beauheim*, 2000a]. After pumping began, 60-mL samples were collected in duplicate from a port at the surface. Sampling frequency varied from minutes to once a day over the duration of the test. Many more samples were collected than were analyzed to ensure that adequate samples were available as needed to define the tracer recovery and breakthrough curves. Samples also were collected from tracer-mixing tanks during injection.

Samples were analyzed for benzoic acids by reverse-phase high-performance liquid chromatography (HPLC) with ultraviolet adsorption detection and for iodide using an ion chromatograph with an ampterometric detector or by HPLC. To measure low concentrations of the benzoic acids and iodide in the Culebra brine, new analysis methodologies were developed [*Farnham et al.*, 2000b]. To evaluate analytical precision, numerous duplicate samples, including blind duplicates, were analyzed. Data from duplicate sample analyses were used to calculate 95% confidence intervals for each data set [*Jones et al.*, 2000]. A time correction was made for all the tracer data to be reported relative to time in the Culebra since start of injection. This correction included subtracting the time for the tracer solution to flow down the tubing in the injection borehole (the approximately 230 m to the Culebra) and back up the tubing in the pumping well to the sampling port. Most times were corrected by between 35 and 75 min; see *Jones* [2000] for additional information on the tubing and borehole volumes

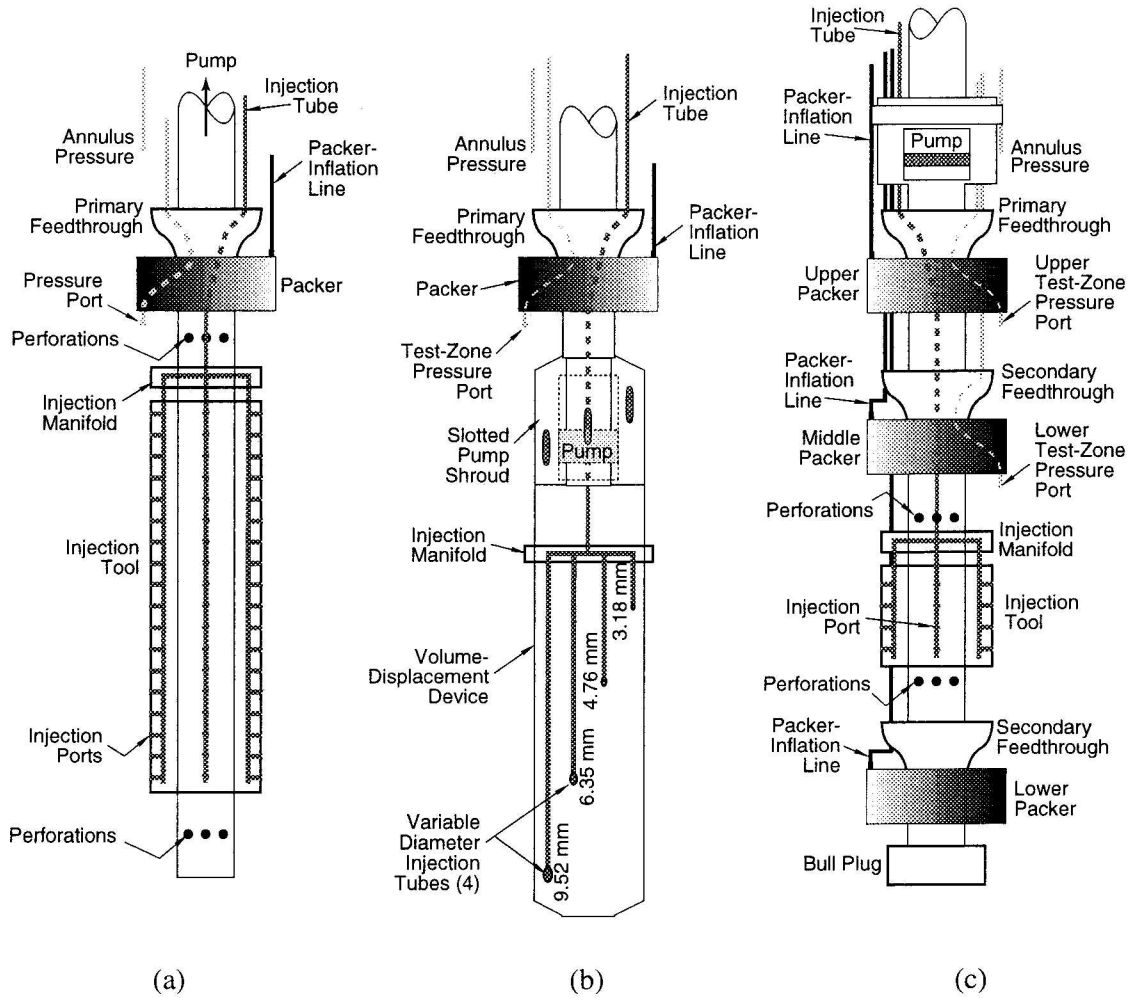

Figure 5. Schematics of the downhole pumping and tracer distribution tools for the (a) H-11, (b) preliminary H-19, and (c) final H-19 single-well injection-withdrawal (SWIW) tests.

(total between 40 and 150 L) used to calculate the time corrections.

6. Tracer Data Observations and Discussion

6.1. SWIW Test Results

Figure 7 shows the tracer recovery curves for the three SWIW tests. The concentration data have been normalized by the concentrations of the injectate solutions as listed in Table 2. Because the injectate concentration is different for different tracers, the normalized tracer concentration detection limit varies between approximately 5×10^{-6} and 2×10^{-5} for the first tracer injected at H-11 and the second tracer injected during the first SWIW test at H-19, respectively. The time is corrected to time since the start of injection of the first tracer. In Figure 7a the data for both the first and the second tracer injected into H-11b1 are shown. Figure 7b shows the data from both the first test conducted at H-19 (SWIW1), which was nearly identical to the H-11 SWIW test, and the second test (SWIW2) for which tracer was only injected into the lower portion of the Culebra. The periods of time for which data are presented are, in part, functions of the injectate concentrations (Table 2). For example, the data set for tracer 2 in Figure 7b terminates sooner than that for tracer 1 at H-19 in part because the concentration falls below the minimum detection limit earlier. For all data sets, if multiple samples were analyzed for a given sampling time, the average value is plotted. The line bounding the data is the 95% confidence interval calculated from numerous duplicate samples [*Jones et al.*, 2000]. The lack of significant data scatter and the tightness of the confidence intervals demonstrates the high precision of the analyses.

Figure 8 shows the normalized cumulative mass recoveries for the first tracers at the H-11 and H-19 hydropads. The mass recoveries are gradual, as would be expected in simulations of a SWIW test in a double-porosity medium [*Tsang*, 1995; *Altman et al.*, 2000]. The late-time ($\geq$100 hours) slopes of the data plotted in Figure 7 vary between approximately -2 and -2.8. These are much shallower slopes than those predicted by *Tsang* [1995] for single-porosity, heterogeneous media. However, the slopes of all five data sets are steeper than the -1.5 late-time log-log slope predicted by conventional double-porosity models for times after the advectively dominated early part of the test and before the diffusion timescale [see *Haggerty et al.*, this issue, section 5.4; *Tsang*, 1995; *Hadermann and Heer*, 1996]. The similarity in the late-time slopes of all five data sets suggests that a similar process is controlling the gradual mass recovery at both hydropads. (See *Haggerty et al.* [this issue] for additional discussion.)

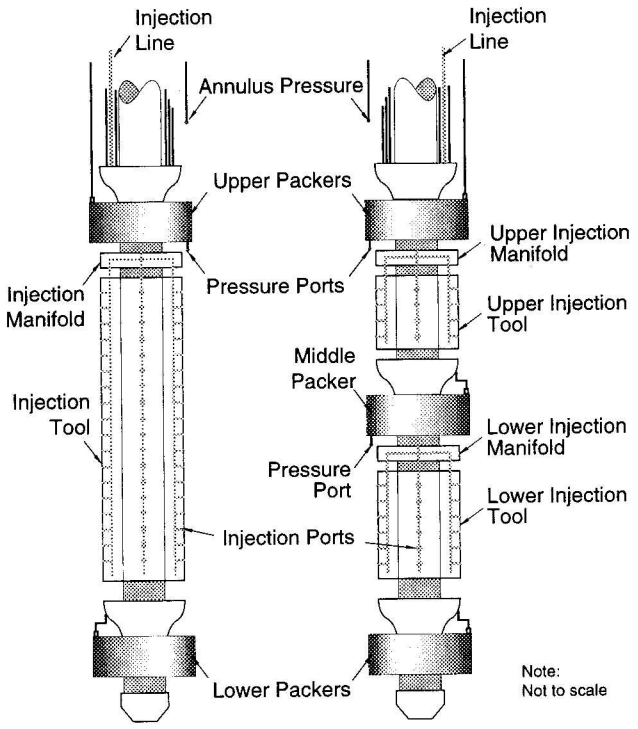

Figure 6. Schematics of the downhole tracer distribution tools for (a) full Culebra thickness injection and (b) partial-thickness or full-thickness injections.

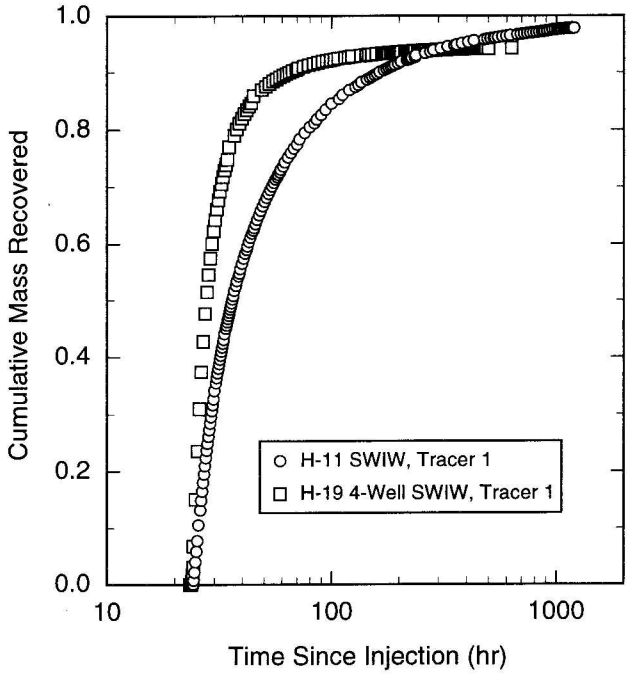

Figure 8. Normalized cumulative mass recovered for the first tracer from the SWIW tests at the H-11 and H-19 hydropads.

6.2. MWCF Test Results

Figure 9 shows the results of the MWCF test at the H-11 hydropad. As was seen in the test conducted in 1988 [*Jones et al.*, 1992; *Meigs et al.*, 2000], the breakthrough curves for the H-11b2 to H-11b1 and H-11b3 to H-11b1 pathways differ dramatically, even though the well separations are approximately the same length. For the lower pumping rate (0.22 L/s) the peak concentration arrives about 20 times faster (0.65 days compared to 12.2 days) and is about 10 times higher for the H-11b3 to H-11b1 path compared to the H-11b2 to H-11b1 path. Similar dramatic differences in breakthrough curves for

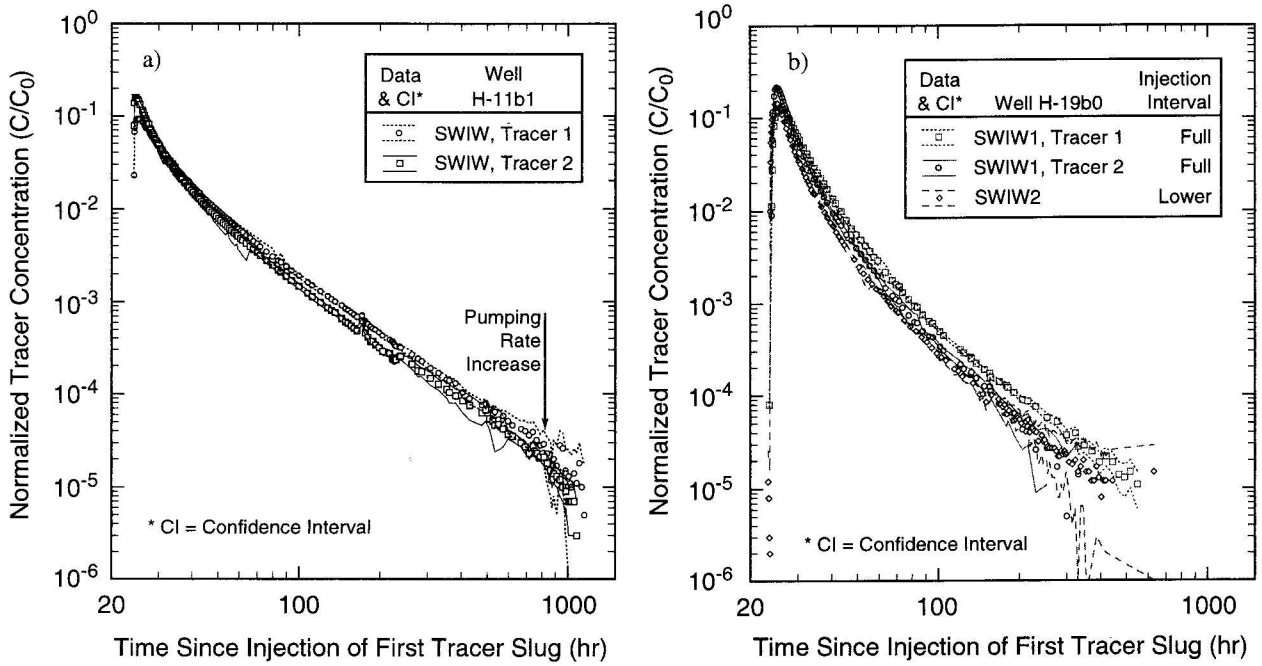

Figure 7. SWIW tracer recovery curves from (a) one test at the H-11 hydropad and (b) two tests at the H-19 hydropad. Here 2,4-DCBA is the tracer for all injections except tracer 2 for H-11 SWIW and H-19 SWIW1; tracers are 3,4-DCBA and o-TFMBA, respectively.

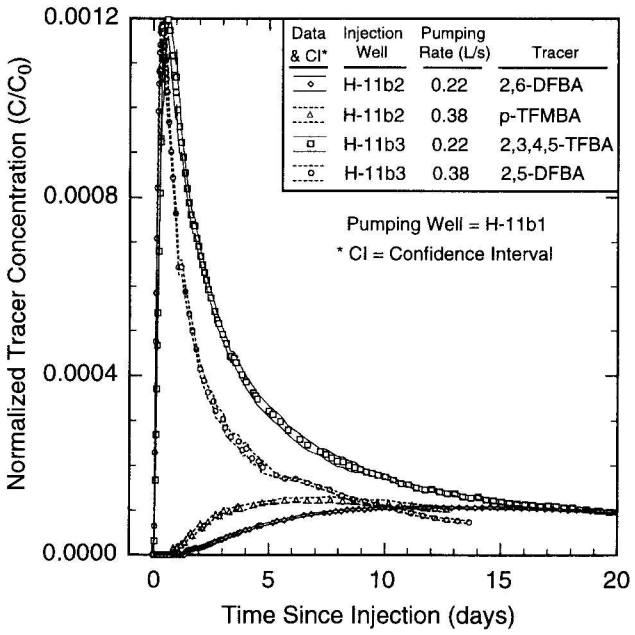

Figure 9. MWCF tracer breakthrough curves from the H-11 hydropad.

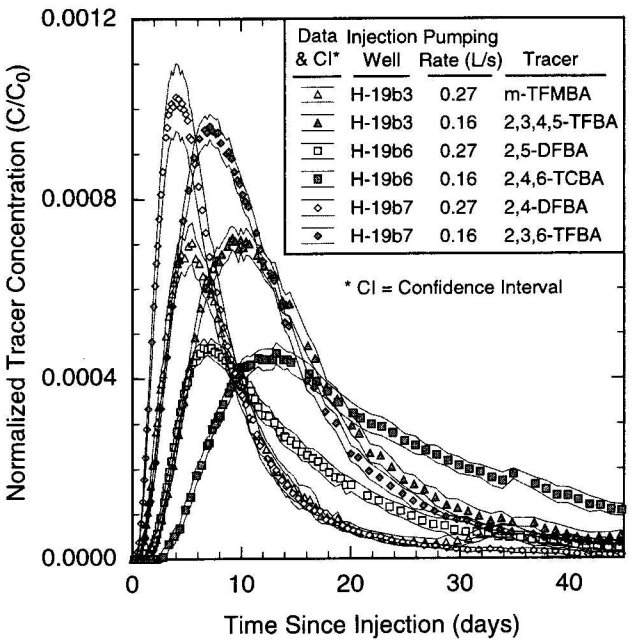

Figure 11. Comparison of MWCF breakthrough curves for tracer injections repeated for two different pumping rates.

different pathways of similar lengths were seen for previous MWCF tracer tests conducted at the H-3 and H-6 hydropads [*Jones et al.*, 1992]. For both pathways at the H-11 hydropad the breakthrough peak heights are approximately the same for both pumping rates. We expected that the data for the lower pumping rate would have a lower peak height resulting from more time for matrix diffusion.

Figure 10 shows the results of the seven-well MWCF test at the H-19 hydropad for the full Culebra interval at the high pumping rate, revealing significant differences in the breakthrough curves that cannot be accounted for by the differences in path lengths alone. For example, the fastest peak arrival time is not from the shortest travel distance, and the slowest peak arrival is not from the longest travel distance. At H-19 the differences between peak arrival times for different pathways of similar lengths are much less dramatic than those found at the H-3, H-6, and H-11 hydropads, suggesting that the Culebra is less heterogeneous (or less anisotropic) at the H-19 hydropad. No pathways were found at the H-19 hydropad with tracer breakthroughs as rapid as those observed at the H-3, H-6, and H-11 hydropads. Given that only two to three pathways were tested at the H-3, H-6, and H-11 hydropads and that six pathways were tested at the H-19 hydropad, the H-19 hydropad apparently lacks the rapid transport pathways found at the other three hydropads.

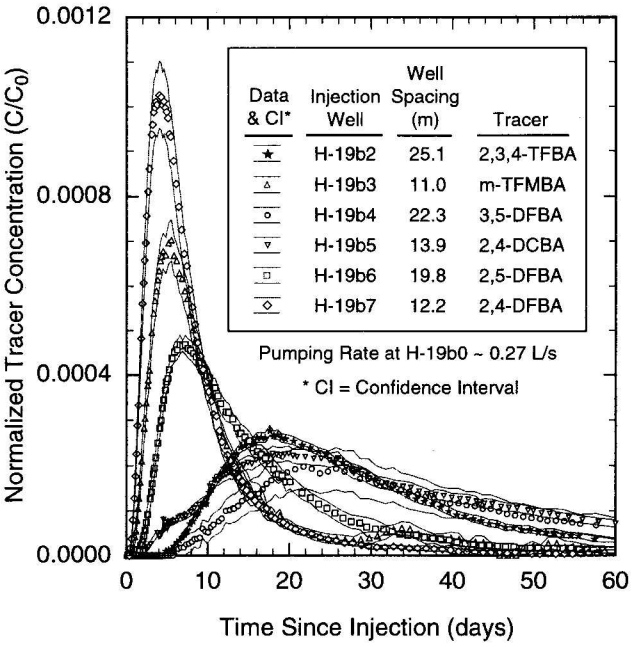

Figure 10. MWCF tracer breakthrough curves from the H-19 hydropad for the full Culebra interval at the high pumping rate.

Figure 11 shows a comparison between breakthrough curves for the three H-19 pathways where tracer injections were repeated while pumping at two different rates during the seven-well test. For each pathway the differences in peak height are not significant when we compare the 95% confidence intervals for the analyses.

Figure 12 shows a comparison of the benzoic acid data and the iodide data for the three pathways for which the pairs of tracers were injected. A lower peak height for the iodide data would be expected if diffusion is an important process because the estimated aqueous diffusion coefficient for iodide is ~2–3 times that of the benzoic acids (Table 3). The peak height of the iodide data from the H-11b3 to H-11b1 pathway (Figure 12a) is clearly lower than the peak height of the benzoic acid data. The iodide peaks also appear to be lower than the benzoic acid peaks for the H-19b3 and H-19b7 to H-19b0 pathways (Figure 12b). However, because of difficulties analyzing iodide in brine, the 95% confidence intervals for the iodide data at H-19 overlap those for the benzoic acid data, which means the apparent differences in peak heights are uncertain.

For three pathways at the H-19 hydropad, injections were

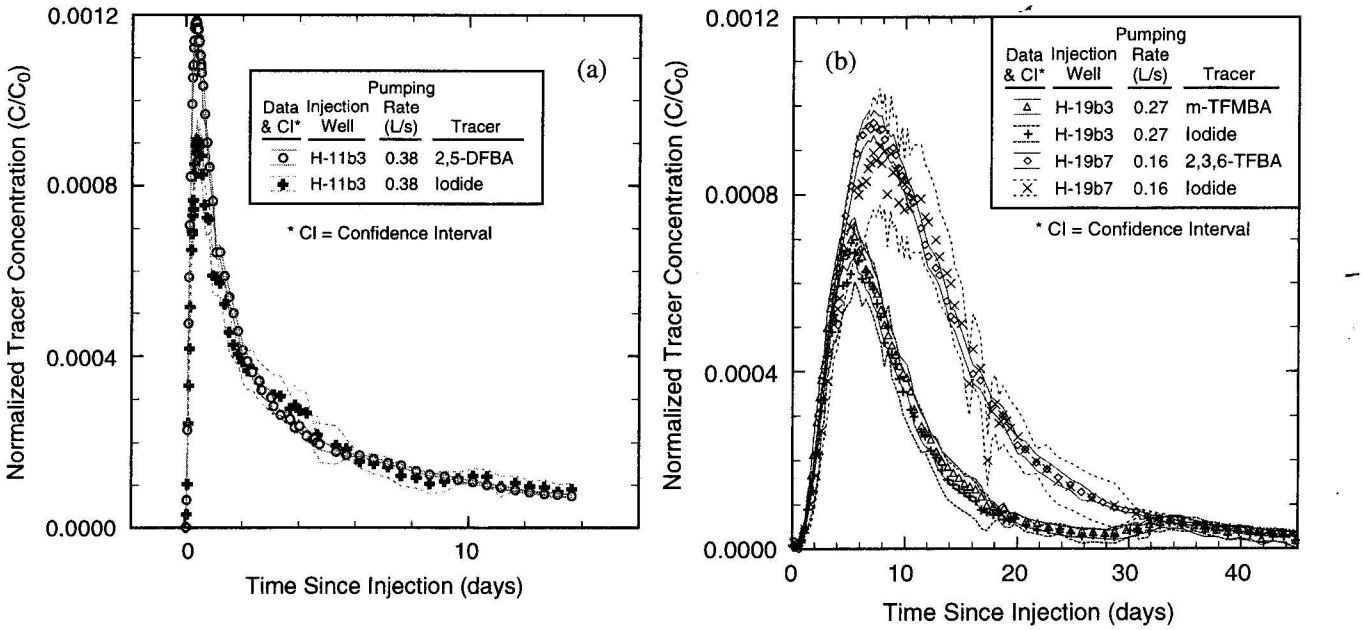

Figure 12. Comparison of benzoic acid and iodide data for (a) one pathway at the H-11 hydropad and (b) two pathways at the H-19 hydropad.

made into packed-off intervals of both the upper and lower Culebra during the seven-well test. The injections into the upper Culebra (CU-1) resulted in very little mass produced at the pumping well (Figure 13 and Table 3). This suggests that the low permeability of the upper Culebra results in extremely slow transport. The injections into the lower Culebra (CU-2 to CU-4) produced breakthrough curves that are quite similar to those from the full-thickness injections (Figure 10). These results suggest that most of the transport of injected tracers is occurring in the lower portion of the Culebra.

Figure 14 shows almost all of the MWCF benzoic acid tracer data from the 1988 and 1996 H-11 tests and the H-19 seven-well test. (See *Meigs et al.* [2000] for details on the 1988 H-11 test.) Injections into the upper Culebra at H-19 are not included in Figure 14b for clarity. The normalized concentration data are plotted versus matrix pore volumes pumped rather than time to facilitate comparison of tracer recoveries from flow paths of different lengths. The matrix pore volumes pumped at any time are defined as the cumulative volume pumped since start of injection divided by the pore volume of a cylinder with a radius equal to the separation between the tracer-injection well and the pumping well, a thickness of 7.4 m, and a porosity of 0.15. Given that tracer is initially distributed in a cylindrical shell around each injection well rather than as a line source, this definition of matrix pore volumes pumped is not rigorously correct. However, it provides a useful metric for comparison of different breakthrough curves.

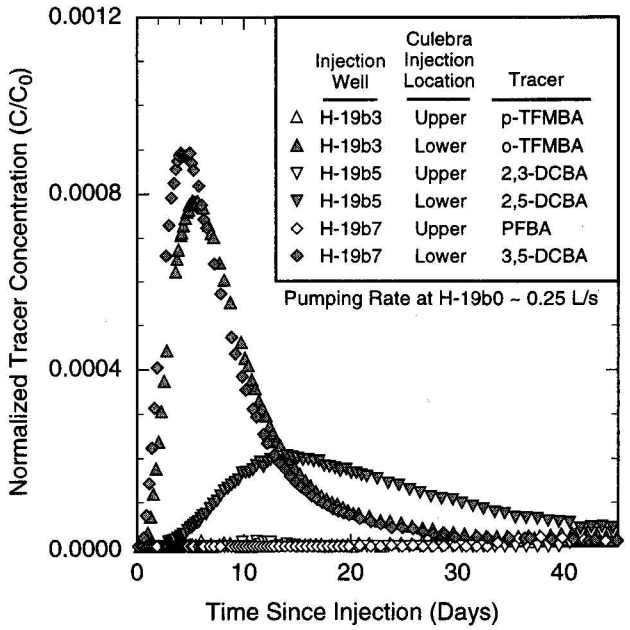

Figure 13. Comparison of injections into the upper and lower Culebra at the H-19 hydropad.

From Figure 14 we see strong similarities among repeated injections along the same pathways, even when the pumping rates differ. This repeatability of experimental results provides confidence in the measurements but also indicates that less-than-twofold differences in pumping rates have little effect on the observed tracer behavior.

All of the tracer breakthrough curves presented in Figure 14 show tracers arriving at the pumping well and reaching their peak concentrations long before even a single matrix pore volume has been pumped. These fast arrivals demonstrate that advection cannot be occurring through the entire matrix pore volume, as defined. Advection must be concentrated in a lower percentage of the porosity and/or a lower percentage of the total Culebra thickness.

At each hydropad the fastest pathways are those for which the fewest matrix pore volumes are pumped before peak concentration is reached. From Figure 14a we see that the H-11b3 to H-11b1 pathway is much faster than the H-11b4 to H-11b1 pathway, even though their azimuths differ by only 13° and that

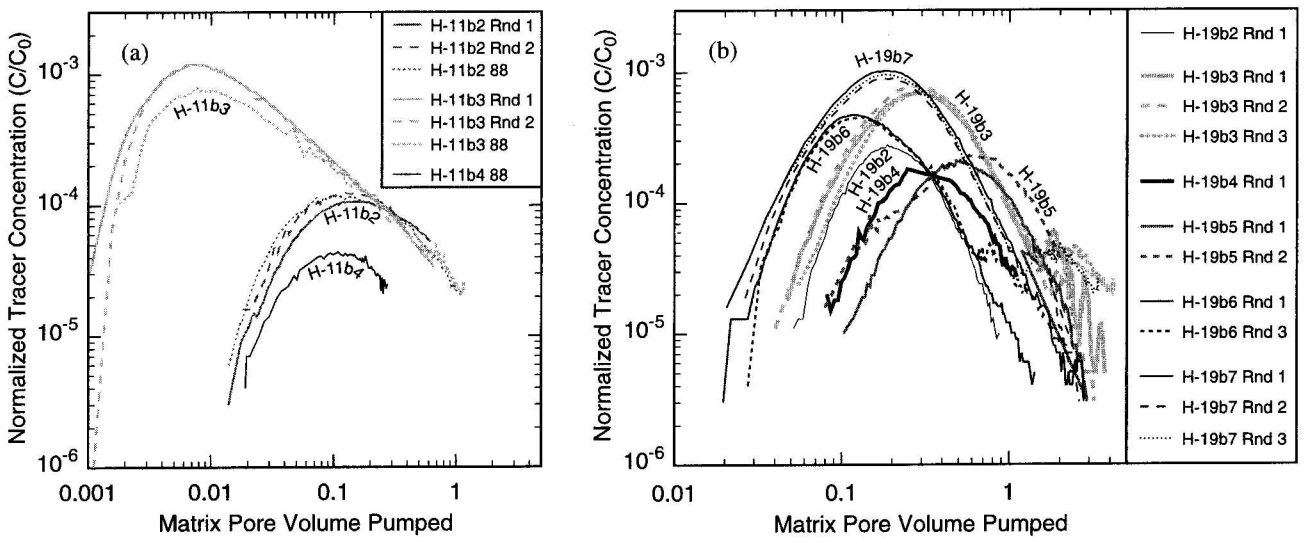

Figure 14. Comparison of MWCF data from all pathways at the (a) H-11 and (b) H-19 hydropads.

the H-11b2 to H-11b1 pathway is the slowest. At the H-19 hydropad the H-19b6 to H-19b0 pathway appears to be the fastest, followed by the H-19b7 and H-19b2 to H-19b0 pathways. These pathways have nearly north-south orientations, with azimuths differing by 2°–13°. The H-19b3 and H-19b4 to H-19b0 pathways are slower and appear to be nearly equivalent. The H-19b5 to H-19b0 is the slowest pathway on the hydropad. At H-19, faster pathways do not always have higher peaks than slower pathways because the well separations and time to peak are sometimes longer, allowing more dilution and diffusion than occurs along some of the slower pathways (compare H-19b6 data to H-19b7 data in Figure 14b). For those pathways that require approximately the same number of matrix pore volumes pumped to reach peak concentrations, the longer pathways always have lower peaks, consistent with increased dilution and diffusion (compare H-19b7 data to H-19b2 data and H-19b3 data to H-19b4 data in Figure 14b.)

Only the fastest pathway on the H-19 hydropad (H-19b6 to H-19b0) was nearly equivalent to the slowest pathway on the H-11 hydropad (H-11b2 to H-11b1) in terms of matrix pore volumes pumped to reach peak concentration. All other H-19 pathways were slower than the slowest H-11 pathway. This observation could be explained by lower advective porosity at H-11 than at H-19. The shapes and late time slopes of the breakthrough curves at the two hydropads are also quite different. The H-11 breakthrough curves tend to be more asymmetric than the H-19 curves, reflecting greater tailing. The late time slopes of the H-19 breakthrough curves are much steeper than the late time slopes of the H-11 curves. These observations are consistent with tracers being released more slowly from the matrix through diffusion at H-11 than at H-19, perhaps reflecting larger matrix blocks at H-11.

7. Summary and Conclusions

The series of tracer tests described in this paper met the goal of producing a detailed and accurate database to evaluate advective and diffusive transport processes in fractured, saturated, permeable media. The lack of significant data scatter and the tight confidence intervals demonstrate the high quality of the tracer analyses.

The data from the three SWIW tests show a gradual mass recovery as would be anticipated if matrix diffusion is the dominant process. The late-time slope of the data is much shallower than was predicted by *Tsang* [1995] for a highly heterogeneous single-porosity system, although it is steeper than the −1.5 log-log slope predicted by a conventional double-porosity model with a single rate of diffusion.

The breakthrough curves from the MWCF tests at the H-11 and H-19 hydropads are quite different, but curves from both sites show gradual mass recovery as would be expected with matrix diffusion. The breakthrough curves for the two different pumping rates had similar peak heights, which appears to be inconsistent with our double-porosity conceptualization. The results of the injection of tracers with two different aqueous diffusion coefficients are somewhat ambiguous in part because of the poor quality of the iodide data from H-19. The H-11 iodide data have a lower peak height than the benzoic acid data, which is consistent with a double-porosity conceptualization. The extremely low mass recoveries for all tracers injected into the upper portion of the Culebra at H-19 indicate that most of the tracer transport is taking place in the lower Culebra. This is consistent with available hydraulic data.

The complexity of the tracer test results suggests that the simple double-porosity conceptual model for transport in the Culebra used to explain past tests [*Jones et al.*, 1992] is overly simplistic. The fact that some of the data appeared to support and other data appeared to contradict the results that would be predicted for a conventional double-porosity medium with a single rate of diffusion led to a detailed reexamination of the Culebra geology [e.g., *Holt*, 1997]. A double-porosity model with a single rate of diffusion is often used to represent a medium in which advection occurs in numerous discrete fractures, based on an assumption that the numerous fractures provide fairly uniform access to all parts of the matrix. Examination of Culebra core does not support an assumption that all parts of the matrix are uniformly accessed by fractures and other advective pathways. The descriptions of *Holt* [1997] of the variations in the porosity structures of the Culebra and recent laboratory diffusion measurements [*Tidwell et al.*, 2000]

also suggest that significant variations in diffusion rates exist within the matrix.

The other papers in this series provide interpretations of a portion of the large data set presented in this paper. *Haggerty et al.* [this issue] show that the SWIW data are consistent with a double-porosity conceptualization of the Culebra if multiple rates of diffusion are incorporated. *McKenna et al.* [this issue] examine a subset of the MWCF tracer test data and demonstrate that a double-porosity model with multiple rates of diffusion provides a fit as good as that provided by a double-porosity model with a single rate of diffusion. Additional efforts to provide a more complete explanation of the data set are in progress. Other researchers are invited to study this data set to improve the understanding of transport processes in fractured, permeable media and test-interpretation methodologies. Additional details on the tracer tests, the data sets, and additional interpretations are presented by *Meigs et al.* [2000]. Electronic versions of the data sets are available from the AGU.

Acknowledgments. We greatly appreciate the assistance of numerous individuals without whose help these tests would not have been possible. Numerous people from INTERA, Inc. (now Duke Engineering and Services) assisted with test design, implementation, and data reduction. Toya Jones provided valuable assistance with test design and the compilation of tracer test information and data such as information in the tables. Joanna Ogintz reduced and organized most of the tracer test data and assisted with compilation of tracer test information. Wayne Stensrud, George Saulnier, John Pickens, Don Fulton, Dave Chace, Curtis Chester, Ronnie Lewis, Kermit Riley, Carl Young, Patricia Johnson, Bryan Bullard, and Bob Coupland assisted with the implementation of the experiment from equipment design and installation to tracer injection and sample collection. Charles Tilburg assisted with some pretest design calculations. Robert Bowman of the New Mexico Institute of Mining and Technology and Irene Farnham and Klaus Stetzenbach of the University of Nevada-Las Vegas (UNLV) provided assistance with selection of tracers. Irene Farnham of UNLV carefully coordinated the analysis of hundreds of samples, assisted by Kaz Lindley, Martha Dominguez, Amy Smiecinski, and Jeannette Daniels of UNLV and Connie Chocas of Sandia National Laboratories (SNL). Yvonne Tsang of Lawrence Berkeley National Laboratory and Ray Ostensen of SNL provided valuable insights for the design of the SWIW tests. Peter Davies of SNL assisted with test design and logistical support. Allan Sattler and Al Lappin of SNL also provided valuable logistical support. Sean McKenna, Susan Altman, James McCord, and Robert Holt of SNL, Roy Haggerty of Oregon State University, and numerous others listed above provided insights into the details of the test data. Tom Corbet, Vince Tidwell, Peter Davies, Ghislain de Marsily, Lenny Konikow, Piotr Maloszewski, Andrzej Zuber, and an anonymous reviewer provided valuable reviews of drafts of the manuscript. Sandia is a multiprogram laboratory operated by Sandia Corporation, a Lockheed Martin Company, for the United States Department of Energy under contract DE-AC04-94AL85000. Electronic versions of the data sets are also available from the first author.

References

Abelin, H., L. Birgersson, J. Gidlund, and I. Neretnieks, A large-scale flow and tracer experiment in granite, 1, Experimental design and flow distribution, *Water Resour. Res.*, *27*(12), 3107–3117, 1991.

Altman, S. J., T. L. Jones, and L. C. Meigs, Controls on mass recovery for single-well injection-withdrawal tracer tests, in *Interpretations of Tracer Tests Performed in the Culebra Dolomite at the Waste Isolation Pilot Plant Site*, edited by L. C. Meigs, R. L. Beauheim, and T. L. Jones, *Rep. SAND97-3109*, chap. 4, pp. 37–68, Sandia Natl. Lab., Albuquerque, N. M., 2000.

Ball, W. P., and P. V. Roberts, Long-term sorption of halogenated organic chemicals by aquifer material, 1, Equilibrium, *Environ. Sci. Technol.*, *25*(7), 1223–1237, 1991.

Beauheim, R. L., Well configurations, test equipment, and hydraulic data, in *Interpretations of Tracer Tests Performed in the Culebra Dolomite at the Waste Isolation Pilot Plant Site*, edited by L. C. Meigs, R. L. Beauheim, and T. L. Jones, *Rep. SAND97-3109*, Append. D, pp. 217–251, Sandia Natl. Lab., Albuquerque, N. M., 2000a.

Beauheim, R. L., Design of H-19 well layout, in *Interpretations of Tracer Tests Performed in the Culebra Dolomite at the Waste Isolation Pilot Plant Site*, edited by L. C. Meigs, R. L. Beauheim, and T. L. Jones, *Rep. SAND97-3109*, Append. G, pp. 267–271, Sandia Natl. Lab., Albuquerque, N. M., 2000b.

Beauheim, R. L., and R. M. Holt, Hydrogeology of the WIPP site, in *Geological and Hydrological Studies of Evaporites in the Northern Delaware Basin for the Waste Isolation Pilot Plant (WIPP), New Mexico, Field Trip #14 Guidebook, November 1–4, 1990, Geological Society of America 1990 Annual Meeting*, pp. 131–179, Dallas Geol. Soc., Dallas, Tex., 1990.

Beauheim, R. L., and G. J. Ruskauff, Analysis of hydraulic tests of the Culebra and Magenta dolomites and Dewey Lake redbeds conducted at the Waste Isolation Pilot Plant site, *Rep. SAND98-0049*, Sandia Natl. Lab., Albuquerque, N. M., 1998.

Beauheim, R. L., L. C. Meigs, and P. B. Davies, Rationale for the H-19 and H-11 tracer tests at the WIPP site, in *Field Tracer Experiments: Role in the Prediction of Radionuclide Migration, Synthesis and Proceeding of an NEA/EC GEOTRAP Workshop, Cologne, Germany, 28–30 August 1996*, pp. 107–118, Organ. for Econ. Coop. Dev., Paris, 1997.

Benson, C. F., and R. S. Bowman, Tri- and tetrafluorobenzoates as nonreactive tracers in soil and groundwater, *Soil Sci. Soc. Am. J.*, *58*(4), 1123–1129, 1994.

Bowman, R. S., and J. F. Gibbens, Difluorobenzoates as nonreactive tracers in soil and ground water, *Ground Water*, *30*(1), 8–14, 1992.

Bradbury, M. H., D. Lever, and D. Kinsey, Aqueous phase diffusion in crystalline rock, *Mater. Res. Soc. Symp. Proc.*, *11*, 569–578, 1982.

Brady, J. B., Intergranular diffusion in metamorphic rocks, *Am. J. Sci.*, *283A*, 181–200, 1983.

Byegård, J., H. Johansson, M. Skålberg, and E.-L. Tullborg, The interaction of sorbing and non-sorbing tracers with different Äspö rock types: Sorption and diffusion experiments in the laboratory scale, *Tech. Rep. TR-98-18*, Swed. Nucl. Fuel and Waste Manage. Co., Stockholm, 1998.

Corbet, T. F., and P. M. Knupp, The role of regional groundwater flow in the hydrogeology of the Culebra Member of the Rustler Formation at the Waste Isolation Pilot Plant (WIPP), southeastern New Mexico, *Rep. SAND96-2133*, Sandia Natl. Lab., Albuquerque, N. M., 1996.

Crawley, M. E., Hydrostatic pressure and fluid density distribution of the Culebra Dolomite Member of the Rustler Formation near the Waste Isolation Pilot Plant, southeastern New Mexico, *Rep. DOE/WIPP 88-030*, Westinghouse Electr. Corp., Carlsbad, N. M., 1988.

Davis, S. N., G. M. Thompson, H. W. Bentley, and G. Stiles, Groundwater tracers—A short review, *Ground Water*, *18*(1), 14–23, 1980.

Farnham, I. M., L. C. Meigs, M. E. Dominguez, K. Lindley, J. M. Daniels, and K. J. Stetzenbach, Evaluation of tracers used for the WIPP tracer tests, in *Interpretations of Tracer Tests Performed in the Culebra Dolomite at the Waste Isolation Pilot Plant Site*, edited by L. C. Meigs, R. L. Beauheim, and T. L. Jones, *Rep. SAND97-3109*, Append. H, pp. 273–289, Sandia Natl. Lab., Albuquerque, N. M., 2000a.

Farnham, I. M., J. M. Daniels, M. E. Dominguez, K. Lindley, K. J. Stetzenbach, and L. C. Meigs, Liquid chromatographic separations of fluoro- and chlorobenzoates used as groundwater tracers, in *Interpretations of Tracer Tests Performed in the Culebra Dolomite at the Waste Isolation Pilot Plant Site*, edited by L. C. Meigs, R. L. Beauheim, and T. L. Jones, *Rep. SAND97-3109*, Append. I, pp. 291–300, Sandia Natl. Lab., Albuquerque, N. M., 2000b.

Foster, S. S. D., The chalk groundwater tritium anomaly—A possible explanation, *J. Hydrol.*, *25*, 159–165, 1975.

Gringarten, A. C. Interpretation of tests in fissured and multilayered reservoirs with double-porosity behavior: Theory and practice, *JPT J. Pet. Technol.*, *36*(4), 549–564, 1984.

Grisak, G. E., J. F. Pickens, and J. A. Cherry, Solute transport through fractured media, 2, Column study of fractured till, *Water Resour. Res.*, *16*(4), 731–739, 1980.

Hadermann, J., and W. Heer, The Grimsel (Switzerland) migration experiment: Integrating field experiments, laboratory investigations and modelling, *J. Contam. Hydrol.*, *21*, 87–100, 1996.

Haggerty, R., S. W. Fleming, L. C. Meigs, and S. A. McKenna, Tracer

tests in a fractured dolomite, 2, Analysis of mass transfer in single-well injection-withdrawal tests, *Water Resour. Res.*, this issue.

Hautojärvi, A., and S. Vuori, Comments on tracer tests and data interpretation, *Rep. TVO/KPA Turvallisuus Ja Tekniikka Työraportti 92-01*, Tech. Res. Cent. of Finland, Nucl. Eng. Lab., Helsinki, 1992.

Holt, R. M., Conceptual model for transport processes in the Culebra Dolomite Member, Rustler Formation, *Rep. SAND97-0194*, Sandia Natl. Lab., Albuquerque, N. M., 1997.

Holt, R. M., and D. W. Powers, Geotechnical activities in the waste handling shaft, Waste Isolation Pilot Plant (WIPP) project, southeastern New Mexico, *Rep. WTSD-TME-038*, Waste Isol. Pilot Plant Off., U.S. Dep. of Energy, Carlsbad, N. M., 1984.

Holt, R. M., and D. W. Powers, Geotechnical activities in the Exhaust Shaft, *Rep. DOE-WIPP 86-008*, Waste Isol. Pilot Plant Proj. Off., U.S. Dep. of Energy, Carlsbad, N. M., 1986.

Holt, R. M., and D. W. Powers, Facies variability and post-depositional alteration within the Rustler Formation in the vicinity of the Waste Isolation Pilot Plant, southeastern New Mexico, *Rep. DOE-WIPP 88-004*, Waste Isol. Pilot Plant Proj. Off., U.S. Dep. of Energy, Carlsbad, N. M., 1988.

Holt, R. M., and D. W. Powers, Geologic mapping of the air intake shaft at the Waste Isolation Pilot Plant, *Rep. DOE-WIPP 90-051*, Waste Isol. Pilot Plant Proj. Off., U.S. Dep. of Energy, Carlsbad, N. M., 1990.

INTERA Technologies, Inc., WIPP Hydrology Program, Waste Isolation Pilot Plant, southeastern New Mexico, *Hydrol. Data Rep. 3*, *Rep. SAND86-7109*, Sandia Natl. Lab., Albuquerque, N. M., 1986.

Jones, T. L., Transport input parameter sheets, in *Interpretations of Tracer Tests Performed in the Culebra Dolomite at the Waste Isolation Pilot Plant Site*, edited by L. C. Meigs, R. L. Beauheim, and T. L. Jones, *Rep. SAND97-3109*, Append. B, pp. 131–168, Sandia Natl. Lab., Albuquerque, N. M., 2000.

Jones, T. L., V. A. Kelley, J. F. Pickens, D. T. Upton, R. L. Beauheim, and P. B. Davies, Integration of interpretation results of tracer tests performed in the Culebra dolomite at the Waste Isolation Pilot Plant site, *Rep. SAND92-1579*, Sandia Natl. Lab., Albuquerque, N. M., 1992.

Jones, T. L., I. M. Farnham, L. C. Meigs, and J. Ogintz, WIPP tracer-test data, in *Interpretations of Tracer Tests Performed in the Culebra Dolomite at the Waste Isolation Pilot Plant Site*, edited by L. C. Meigs, R. L. Beauheim, and T. L. Jones, *Rep. SAND97-3109*, Append. C, pp. 169–216, Sandia Natl. Lab., Albuquerque, N. M., 2000.

Kelley, V. A., and G. J. Saulnier Jr., Core analyses for selected samples from the Culebra dolomite at the Waste Isolation Pilot Plant site, *Rep. SAND90-7011*, Sandia Natl. Lab., Albuquerque, N. M., 1990.

Klinkenberg, L. J., Analogy between diffusion and electrical conductivity in porous rocks, *Geol. Soc. Am. Bull.*, *62*, 559–564, 1951.

LaVenue, A. M., T. L. Cauffman, and J. F. Pickens, Ground-water flow modeling of the Culebra dolomite, in *Model Calibration*, vol. I, *Rep. SAND89-7068/1*, Sandia Natl. Lab., Albuquerque, N. M., 1990.

Lessoff, S. C., and L. F. Konikow, Ambiguity in measuring matrix diffusion with single-well injection/recovery tracer tests, *Ground Water*, *35*(1), 166–176, 1997.

Lever, D. A., M. H. Bradbury, and S. J. Hemingway, Modeling the effects of diffusion into the rock matrix on radionuclide migration, *Prog. Nucl. Energy*, *12*(1), 85–115, 1983.

Maloszewski, P., and A. Zuber, Tracer experiments in fractured rocks: Matrix diffusion and the validity of models, *Water Resour. Res.*, *29*(8), 2723–2735, 1993.

McKenna, S. A., L. C. Meigs, and R. Haggerty, Tracer tests in a fractured dolomite, 3, Double-porosity, multiple-rate mass transfer processes in multiwell convergent-flow tracer tests, *Water Resour. Res.*, this issue.

Meigs, L. C., and R. L. Beauheim, Characteristics of the Culebra, in *Interpretations of Tracer Tests Performed in the Culebra Dolomite at the Waste Isolation Pilot Plant Site*, edited by L. C. Meigs, R. L. Beauheim, and T. L. Jones, *Rep. SAND97-3109*, chap. 2, pp. 9–15, Sandia Natl. Lab., Albuquerque, N. M., 2000.

Meigs, L. C., R. L. Beauheim, J. T. McCord, Y. W. Tsang, and R. Haggerty, Design, modelling, and current interpretations of the H-19 and H-11 tracer tests at the WIPP site, in *Field Tracer Experiments: Role in the Prediction of Radionuclide Migration Synthesis and Proceedings of an NEA/EC Workshop, Cologne, Germany, 28–30 August 1996*, pp. 157–169, Organ. for Econ. Coop. Dev., Paris, 1997.

Meigs, L. C., T. L. Jones, and R. L. Beauheim (Eds.), Interpretations of tracer tests performed in the Culebra dolomite at the Waste Isolation Pilot Plant site, *Rep. SAND97-3109*, Sandia Natl. Lab., Albuquerque, N. M., 2000.

Mercer, J. W., and B. R. Orr, Interim data report on the geohydrology of the proposed Waste Isolation Pilot Plant site in southeastern New Mexico, *U.S. Geol. Surv. Water Resour. Invest. Rep. 79-98*, 1979.

Mercer, J. W., D. L. Cole, and R. M. Holt, Basic data report for drillholes on the H-19 hydropad, Waste Isolation Pilot Plant, *Rep. SAND98-0071*, Sandia Natl. Lab., Albuquerque, N. M., 1998.

Moench, A. F., Convergent radial dispersion in a double-porosity aquifer with fracture skin: Analytical solution and application to a field experiment in fractured chalk, *Water Resour. Res.*, *31*(8), 1823–1835, 1995.

Moreno, L., I. Neretnieks, and T. Eriksen, Analysis of some laboratory runs in natural fissures, *Water Resour. Res.*, *21*(7), 951–958, 1985.

National Research Council, *Alternatives for Groundwater Cleanup*, Natl. Acad. Press, Washington, D. C., 1994.

Neretnieks, I., Diffusion in the rock matrix: An important factor in radionuclide retardation?, *J. Geophys. Res.*, *85*(B8), 4379–4397, 1980.

Neretnieks, I., Age dating of groundwater in fissured rock: Influence of water volume in micropores, *Water Resour. Res.*, *17*(2), 421–422, 1981.

Neretnieks, I., Solute transport in fractured rock—Applications to radionuclide waste repositories, in *Flow and Contaminant Transport in Fractured Rock*, edited by J. Bear, C.-F. Tsang, and G. de Marsily, Academic, San Diego, Calif., 1993.

Novakowski, K. S., and P. A. Lapcevic, Field measurement of radial solute transport in fractured rock, *Water Resour. Res.*, *30*(1), 37–44, 1994.

Randall, W. S., M. E. Crawley, and M. L. Lyon, 1988 annual water quality data report for the Waste Isolation Pilot Plant, *Rep. DOE-WIPP 88-006*, Westinghouse Electr. Co., Carlsbad, N. M., 1988.

Schackelford, C. D., Laboratory diffusion testing for waste disposal—A review, *J. Contam. Hydrol.*, *7*, 177–217, 1991.

Siegel, M. D., and S. A. Anderholm, Geochemical evolution of groundwater in the Culebra dolomite near the Waste Isolation Pilot Plant, southeastern New Mexico, USA, *Geochim. Cosmochim. Acta*, *58*, 2299–2323, 1994.

Siegel, M. D., K. L. Robinson, and J. Myers, Solute relationships in groundwaters from the Culebra dolomite and related rocks in the Waste Isolation Pilot Plant area, in *Hydrogeochemical Studies of the Rustler Formation and Related Rocks in the Waste Isolation Pilot Plant Area, Southeastern New Mexico*, edited by M. D. Seigel, S. J. Lambert, and K. L. Robinson, *Rep. SAND88-0196*, pp. 2-1–2-164, Sandia Natl. Lab., Albuquerque, N. M., 1991.

Skagius, K., and I. Neretnieks, Porosities and diffusivities of some nonsorbing species in crystalline rocks, *Water Resour. Res.*, *22*(3), 389–398, 1986.

Skagius, K., and I. Neretnieks, Measurements of cesium and strontium diffusion in biotite gneiss, *Water Resour. Res.*, *24*(1), 75–84, 1988.

Stensrud, W. A., M. A. Bame, K. D. Lantz, J. B. Palmer, and G. J. Saulnier Jr., WIPP Hydrology Program, Waste Isolation Pilot Plant, southeastern New Mexico, *Hydrol. Data Rep. 8*, *Rep. SAND89-7056*, Sandia Natl. Lab., Albuquerque, N. M., 1990.

Tidwell, V. C., L. C. Meigs, T. L. Christian-Frear, and C. M. Boney, Effects of spatially heterogeneous porosity on matrix diffusion as investigated by X-ray absorption imaging, *J. Contam. Hydrol.*, *42*, 285–302, 2000.

Tsang, Y. W., Study of alternative tracer tests in characterizing transport in fractured rocks, *Geophys. Res. Lett.*, *22*(11), 1421–1424, 1995.

Tucker, W. A., and L. H. Nelken, Diffusion coefficients in air and water, in *Handbook of Chemical Property Estimation Methods*, edited by W. J. Lyman, W. R. Reehl, and D. H. Rosenblatt, pp. 17-1–17-25, McGraw-Hill, New York, 1982.

U.S. Department of Energy, Title 40 CFR Part 191 compliance certification application for the Waste Isolation Pilot Plant, vol. I, *Rep. DOE/CAO-1996-2184*, Waste Isol. Pilot Plant Off., U.S. Dep. of Energy, Carlsbad, N. M., 1996.

Volckaert, G., and A. Gautschi, Field tracer experiments in clay, in *Field Tracer Experiments: Role in the Prediction of Radionuclide Migration, Synthesis and Proceeding of an NEA/EC GEOTRAP Workshop, Cologne, Germany, 28–30 August 1996*, pp. 95–101, Organ. for Econ. Coop. Dev., Paris, 1997.

Wels, C., L. Smith, and T. T. Vandergraaf, Influence of specific surface area on transport of sorbing solutes in fractures: An experimental analysis, *Water Resour. Res.*, *32*(7), 1943–1954, 1996.

Wood, W. W., Diffusion: The source of confusion?, *Ground Water*, *34*(2), 193, 1996.

Wood, W. W., T. F. Kraemer, and P. P. Hearn Jr., Intragranular diffusion: An important mechanism influencing solute transport in clastic aquifers?, *Science*, *247*(4950), 1569–1572, 1990.

R. L. Beauheim, Repository Performance and Certification Department, Sandia National Laboratories, P.O. Box 5800, MS 1395, Albuquerque, NM 87185-1395. (rlbeauheim@sandia.gov)

L. C. Meigs, Geohydrology Department, Sandia National Laboratories, P.O. Box 5800, MS 0735, Albuquerque, NM 87185-0735. (lcmeigs@sandia.gov)

(Received March 17, 2000; revised October 13, 2000; accepted October 13, 2000.)